Materials and Design 46 (2013) 8–15

Contents lists available at SciVerse ScienceDirect

Materials and Design

journal homepage: www.elsevier.com/locate/matdes

Technical Report

Finite element modelling of α particle size on the stress strain curve of near beta Ti alloy

G. Srinivasu [a,*], R.N. Rao [a], T.K. Nandy [b], D.K. Gupta [b]

[a] Mechanical Engineering Department, National Institute of Technology Warangal, India
[b] Defence Metallurgical Research Laboratory, Hyderabad, India

ARTICLE INFO

Article history:
Received 4 July 2012
Accepted 15 September 2012
Available online 12 October 2012

ABSTRACT

In the present study the stress–strain curve of low cost near β titanium alloy (Ti–10V–4.5Fe–3Al) at 16% volume fraction of α was measured. Also, it was simulated to be based on the stress–strain curves of individual phases both α and β by using Finite Element Method (FEM), then measured result compared with the calculated curve. The average error between the predicted and measured one is 6.22% and coefficient of correlation (*R*) is 0.98, these results showed that the simulated results closely fit the measured one, which proves that this FEM model used in this work is appropriate. The distributions of stress and strain are also discussed with the help of FEM model. Additionally, an attempt was made to study the effect of α particle size on the stress–strain curve for the same alloy (16% volume fraction of α). As a result the α particle size increases, then the stress–strain curve is shifted down. The distributions of stress and strain are also discussed for different α particle sizes.

1. Introduction

Titanium (Ti) alloys having a unique combination of mechanical and physical properties and excellent corrosion resistance to sea water and other chloride media, which make them popular for a variety of applications [1]. Titanium alloys are excellent candidates for aerospace applications owing to their high strength to weight ratio and excellent corrosion resistance [2]. The expansion of titanium applications to non-aerospace industries like automotive, chemical, energy, marine, biomedical, sports, and architecture entails improvements in the understanding of titanium metallurgy, advances in processing methods, ability to manufacture components without defects, and development of low cost alloys [3]. Beta titanium alloys offer a wide range of mechanical and chemical properties and can be thermo-mechanically processed to achieve high strength, toughness and fatigue resistance even in large sections [4]. But the cost of β titanium alloys is very high. Hence low cost β titanium alloys are coming into the present scenario. The development of a low cost beta (LCB) alloy [5] like Timetal LCB (Ti–4.5Fe–6.8Mo–1.5Al) makes use of ferromolybdenum addition to reduce the cost so that it becomes competitive for automobile and other aerospace applications. The alloy possesses excellent workability and mechanical properties which are comparable to that of high strength steel [6]. Now many of the researchers concentrated on the development and property evaluation of a low cost β titanium alloys [7–10].

The microstructure is one of the important factors that controlling both the tensile and fatigue strength which are important criteria of material service capabilities both in aerospace and industrial applications. With different percentages of α and β phases, several metastable microstructures can be formed. Thus, it is formed with the integration of several physical properties, functional performances, and strain in different phases and even in different grains is inhomogeneous; it is hard to express the distribution of stress and strain in the titanium alloy clearly [11]. Therefore, any innovation in the design and predicting the properties with the help of the microstructure will lead to reduce experimentation and large overall cost savings. The key to these innovations is a thorough understanding of the material's constitutive response to the imposed conditions and detailed process analysis. This is achieved by effective material modelling and integration of microstructural information with process simulation and optimisation methodologies.

For modelling of material properties, different soft computing techniques are available. In that Finite Element Method (FEM) is one of the most widely used technique for modelling of material properties like tensile properties [12] and fracture toughness properties [13,14]. FEM is used not only in room temperature but also in high temperature conditions [15]. Many investigators [16,17] calculated the stress–strain curve and then compared with the measured one, by using the stress–strain curves of the individual phases. But the literature available in this particular area is limited. In this paper the stress–strain curve of 0.16α of Ti alloy calculated based on the individual stress–strain curves of single α and β phase alloys using Finite Element Method (FEM). The simulated result was compared with the measured one and then, the distribution

* Corresponding author. Tel.: +91 9493040920.
E-mail addresses: srinivasu@nitw.ac.in, nivassetti@gmail.com (G. Srinivasu).

0261-3069/$ - see front matter © 2012 Elsevier Ltd. All rights reserved.
http://dx.doi.org/10.1016/j.matdes.2012.09.047

Table 1
Chemical composition of the Ti–10V–4.5Fe–3Al alloy.

	Elements (wt%)								
	V	Al	Fe	O	N	P	C	S	Ti
Ti–10V–4.5Fe–3Al	9.6–10	3–3.2	4–5	0.11	0.009	0.01	0.02	0.001	Rest

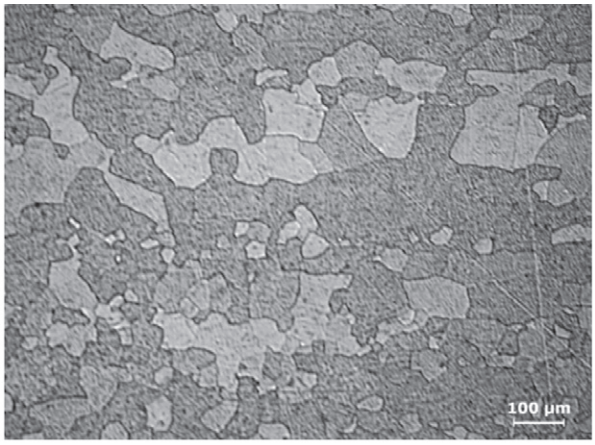

(a) Optical Microstructure for β ST

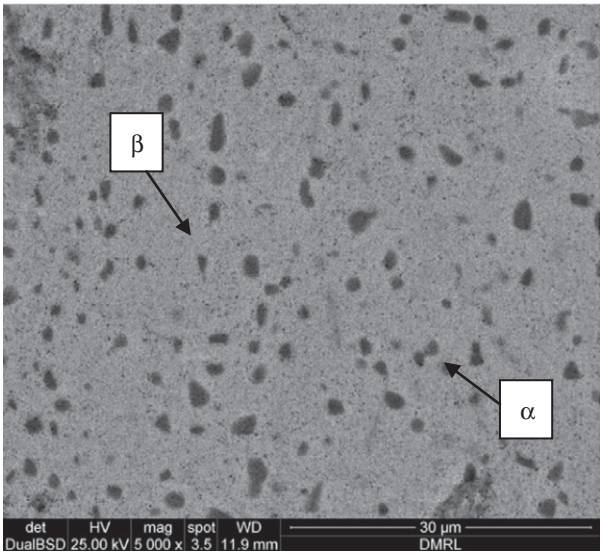

(b) Scanning Electron Micrograph for α + β ST

Fig. 1. Micrographs of Ti–10V–4.5Fe–3Al alloy.

of stress and strain of the 0.16α of Ti–10V–4.5Fe–3Al alloy was analysed in this work. Finally, with the FEM model the effect of secondary phase (α) particle size on the stress–strain curve is calculated.

2. Materials and methods

2.1. Materials and experimental procedure

The LCB Ti alloy (Ti–10V–4.5Fe–3Al) was used in the present work and it was developed in vacuum arc re-melting (VAR) furnace. Table 1 shows the chemical composition of the alloy. The β transus temperature of the alloy (T_β) was determined is 780 °C in close agreement with the value of the β transus for the alloy as per Yolton's formula [18]. The alloy processed thermo-mechanically (Forging and Rolling) in order to get the equi axed α particles in β phase. Thermo-mechanical process includes forging and rolling as previously mentioned. The ingot was forged at 900 °C (β forging) in order to remove the defects in the ingot. Further it was rolled into 10 mm thick slab at 750 °C (α–β rolling).

The tensile samples of suitable length cut from the rolled slab in the longitudinal orientation were subjected solution treated in β (800 °C), and α + β (750 °C) conditions. Fig. 1 shows the microstructure of the alloy at two solution treatment temperatures. The heat treatment was carried out in an electrical heat treatment furnace using Kanthal as the heating element. For microstructural examination, samples were cut from the 10 mm thick slab, and heat treated with the tensile specimens at required conditions, polished

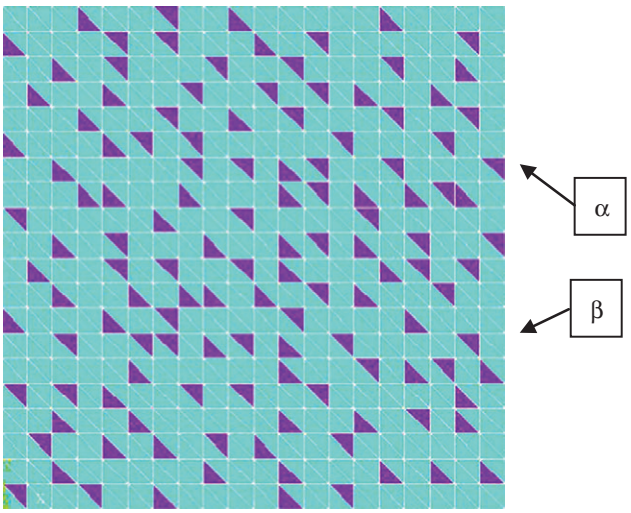

Fig. 2. FEM model (16% volume fraction of α).

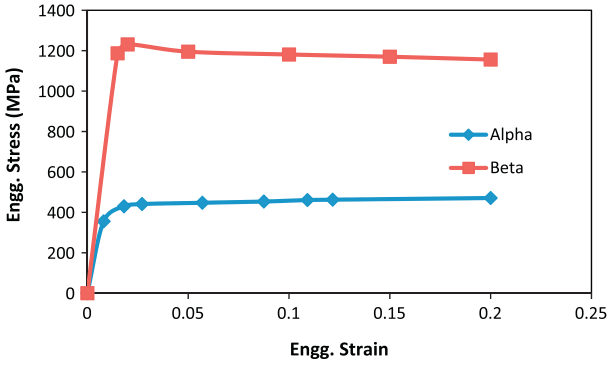

Fig. 3. Stress–strain curves of single phase β and single phase α.

Table 2
Input data used for simulation.

Sl. no.	Single phase β		Single phase α	
	Strain	Stress (MPa)	Strain	Stress (MPa)
1	0.015	1187	0.008055	355.5
2	0.02	1231	0.018157	430
3	0.05	1195	0.027105	441
4	0.1	1181	0.087515	454
5	0.15	1170	0.121644	463
6	0.2	1156	0.2	471

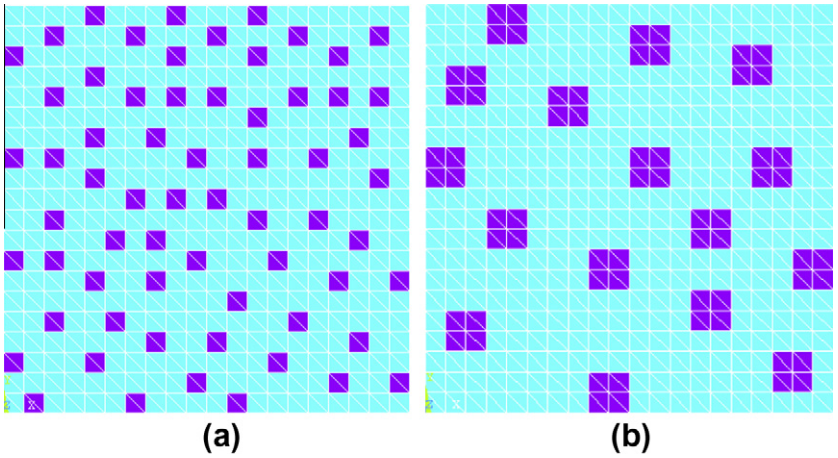

Fig. 4. Microstructural FE Models with different grain sizes of α; (a) medium (b) coarser.

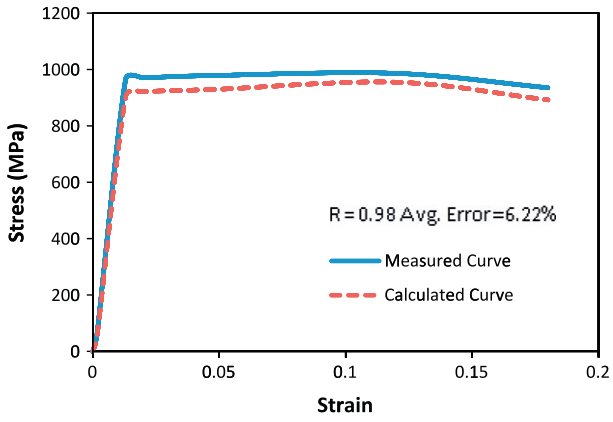

Fig. 5. Comparison between the measured and calculated stress–strain curve.

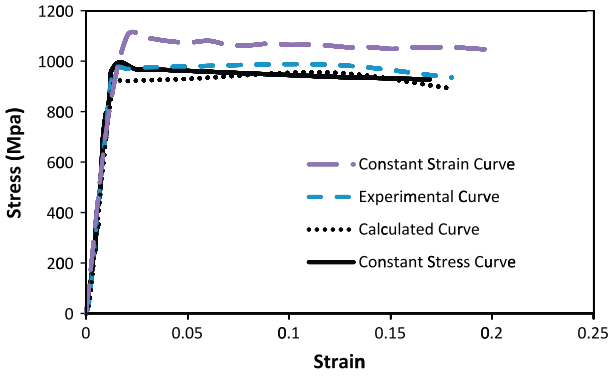

Fig. 6. Comparison of calculated and measured stress–strain curves with constant stress curve and constant strain curve for 16% of volume fractions of α.

metallographically using standard metallographic technique and finally etched with Kroll's reagent (2 ml of HF, 6 ml of HNO_3, 92 ml of Distilled Water). Etched samples were examined under scanning electron microscopy and optical microscope. The tensile tests were carried out according ASTM E8M-97 in screw-driven digital control INSTRON® 5500R test system in order to obtain the stress–strain curves.

2.2. Finite element modelling

A Finite Element (FE) 2-Dimensional (2D) model was developed in Ansys 10 software. The FE model is the replica of the microstructure in Fig. 1a. The 2D FE model consists of 800 triangular elements which are connected with 1681 nodes. The 2D model developed according to the microstructure of α + β solution treated condition. Initially the model used for the prediction of stress–strain curve consist of 162 triangular elements, but predicted results shows high average error. In order to achieve the convergence solution, the number of elements elements is increased from 162 to 968 by keeping the volume fraction of α is constant. At 800 elements the model started giving the convergence solution. Once the number of elements is optimised, then the model is used for prediction of stress–strain curve. Fig. 2 shows the 2D FEM model, here the green triangles represents β phase and violet triangles represents α phase. In order to simulate the stress–strain curve, the model requires input material properties of individual phases both α and β. Fig. 3 shows the stress–strain curves of the both individual phases α and β (Table 2). The Young's modulus of α and β phases are 45,125 MPa and 79,524 MPa respectively. The β stress–strain curve is determined experimentally, and the α curve is obtained from the literature [20]. Bottom of the model is constrained in *X* and *Y* directions and the loads are applied in terms of displacements (0.005, 0.05, 0.1, 0.15 and 0.2 mm) at the top portion.

Additionally, in present the work attempts have been made to determine the effect of α particle size on the stress strain curve. Fig. 4 shows the FEM models with two different α particles sizes (which refers to the medium and coarser size) bigger than the α particles size in Fig. 2 (refers to smaller size). The input stress–strain curves of both individual phases both α and β for the corresponding FEM models of medium and coarser α particle size are calculated based on Hall Petch relations. The Hall Petch relations for both the phases are mentioned below.

Hall Petch relation for α is

$$\sigma_y = 0.2275(D^{-0.5}) + 228.92 \quad (1)$$

Hall Petch relation for β is

$$\sigma_y = 1.383(D^{-0.5}) + 731.04 \quad (2)$$

where σ_y is the yield stress in MPa and *D* is the grain size in m (α or β).

3. Results and discussions

3.1. Microstructure

Fig. 1 shows the representative microstructure of the alloy solution treated at β (800 °C/1 h), and α + β (750 °C/4 h) conditions

followed by water quenching. Fig. 1a shows the β grains and the average grain size is 97.34 ± 13.37 μm. It is observed from Fig. 1b that equi axed α particles are distributed in the continuous β matrix. The volume fraction of α phase (black) is around 16% and the remaining is β.

3.2. Comparison between the measured and simulated stress–strain curves

By using Ansys 10, the stress–strain curve of the present alloy at 16% volume fraction of α calculated based on the individual stress–strain curves of both α and β phases. The measured curve and simulated curve calculated by a 2D FEM model are shown in Fig. 5. The average error between the predicted and measured stress–strain curve is 6.22% and the coefficient of correlation (R) is 0.98 and it was calculated with the help of Eq. (3), but the fit is acceptable. Therefore, the FEM used in this work is correct, which can be used for further simulations to know the effect of α particle size on the stress–strain curve.

Similar observations are reported in titanium alloys [11] and other alloy systems [16,20]. Four principal reasons have been attributed to this behaviour [16]:

(i) The modelling has been carried out in two dimensional while the material deformation is a three dimensional phenomenon.

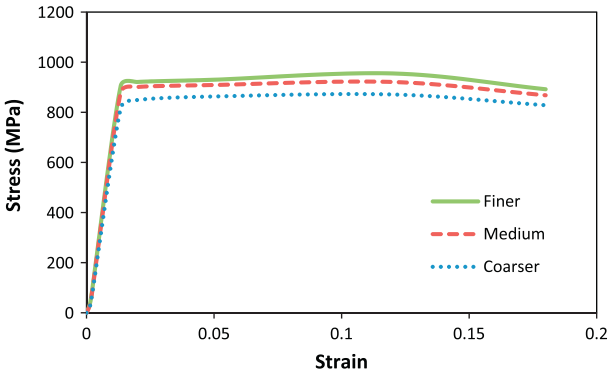

Fig. 8. Comparison of calculated stress–strain curves at different grain sizes of α.

(ii) The behaviour of the interface between α and β has not been incorporated in the model. It is expected that the interface region which as a finite thickness/volume will be harder than both α and β.

(iii) The α stress–strain curve has been taken from the work of Ankem et al. [19] which is based on Ti–Mn system. For the present work, the composition of α contains Al and V will be different and therefore the stress–strain curve is expected to be different.

(iv) Size of α particles is considerably fine (14–19 μm) leading to a different stress–strain behaviour from that of Ankem et al. [19].

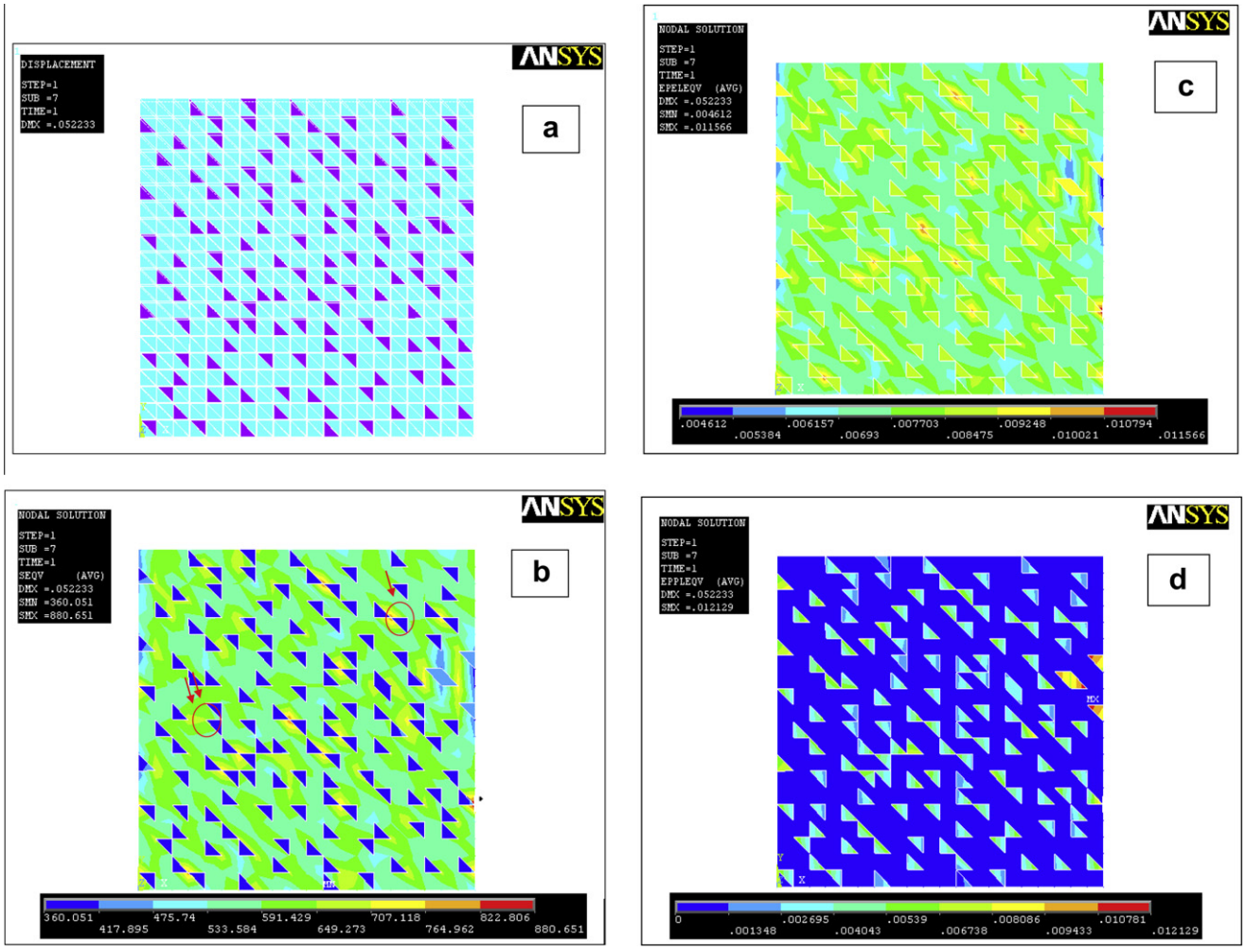

Fig. 7. Distributions of Ti alloy (16% volume fraction of α) at 0.05 mm load (a) deformation, (b) VonMises stress (c) VonMises elastic strain, (d) VonMises plastic strain.

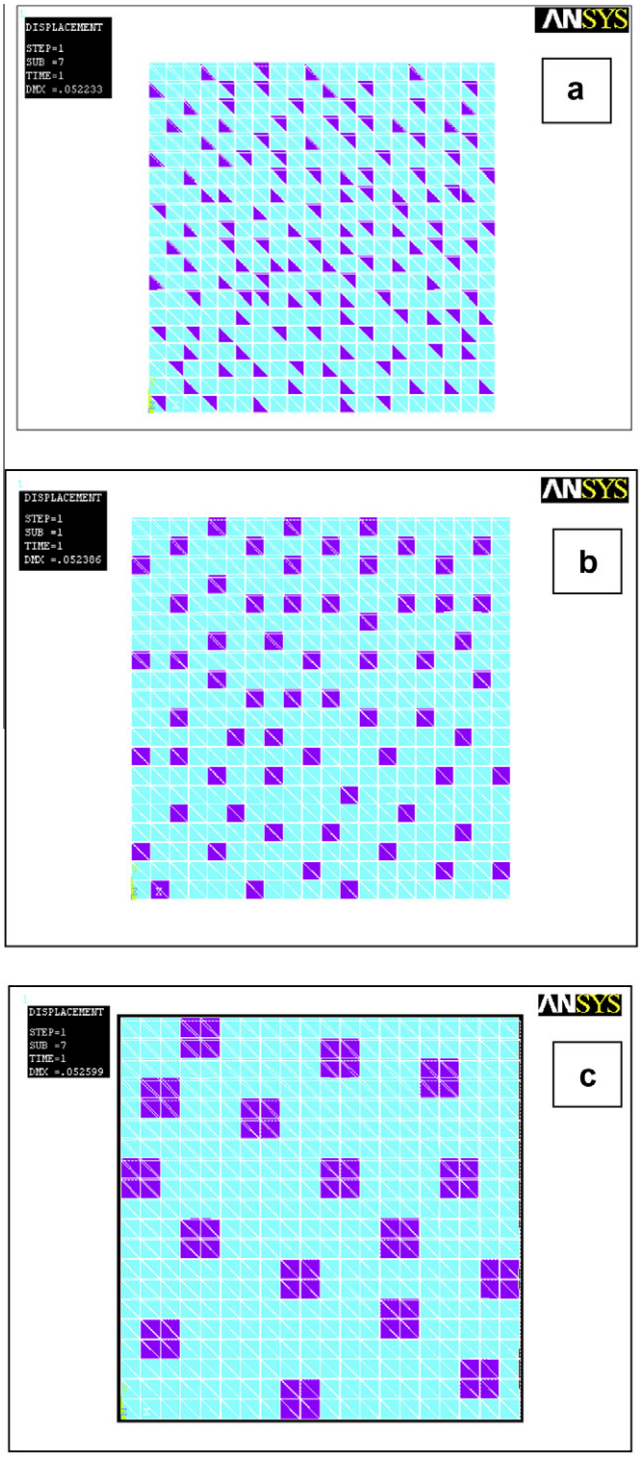

Fig. 9. Deformations at 0.83% strain for (a) finer, (b) medium and (c) coarser α grain sizes.

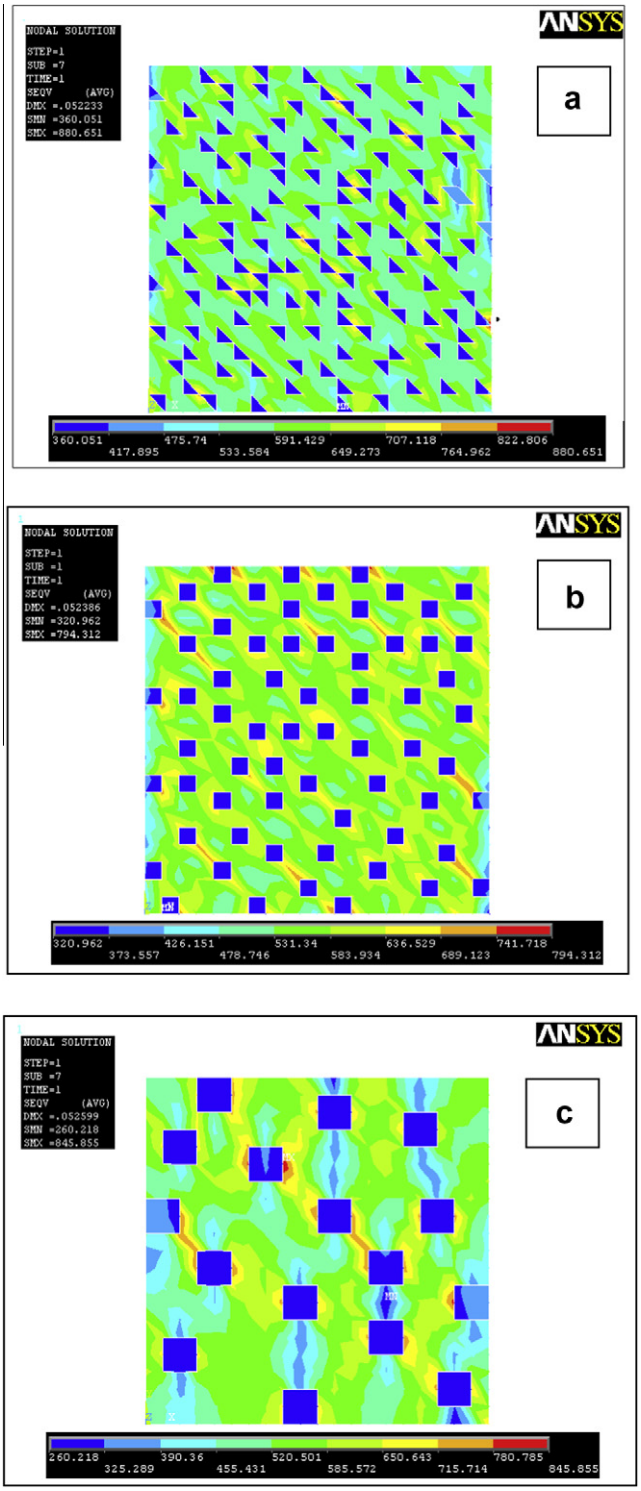

Fig. 10. VonMises stress distributions at 0.83% strain for (a) finer, (b) medium and (c) coarser α grain sizes.

$$R = \frac{(n\sum xy) - (\sum x \sum y)}{\sqrt{n\sum x^2 - (\sum x)^2}\sqrt{n\sum y^2 - (\sum y)^2}} \quad (3)$$

where x is the experimental stress value; y the predicted stress value and n is the number of data points.

Fig. 6 shows the experimental and fitted curves along with the constant stress and constant strain curves. For 16% volume fractions of α (Fig. 6), both predicted and experimental curves overlap with constant stress curves. This is in contrast to the results of Ti–8Mn [19] where the predicted curve is closer to that of the constant strain curve. Thus, in the present work, it appears that the deformation of two phase alloy is better represented as constant stress behaviour. This correlated from the stress–strain map shown in Fig. 7d.

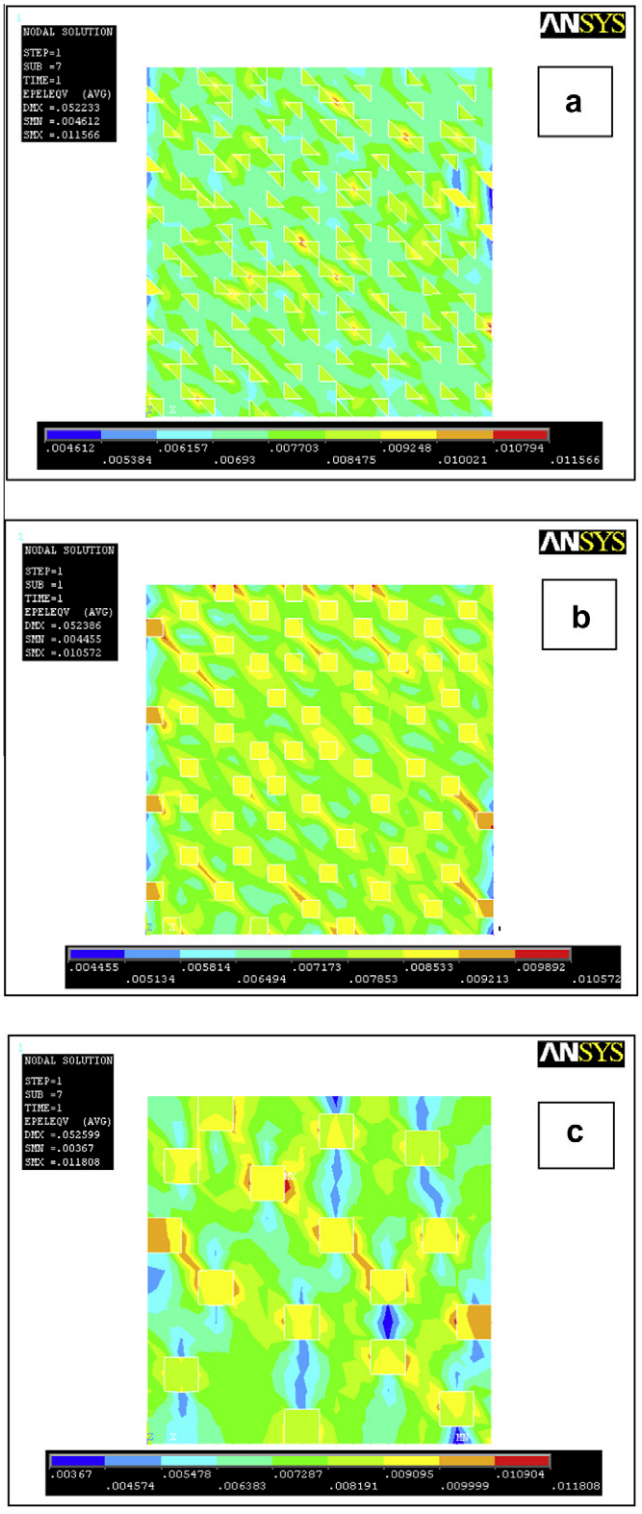

Fig. 11. VonMises elastic strain distributions at 0.83% strain for (a) finer, (b) medium and (c) coarser α grain sizes.

3.3. The analysis of the distribution of the stress and strain of the titanium alloy

Element deformation map for 0.83% strain (0.05 mm displacement) is shown in Fig. 7a for 16% volume fractions of α. The original model (without deformation) is also plotted. Displacement of the elements at the top with respect to the original model is varies as a function of location while those at the bottom are not displaced. This is expected, since the bottom surface in the model (axi symmetry) used has been kept stationary (rigid). The stress map is shown in Fig. 7b for 16% volume fractions of α. Firstly, the stress values are higher in β phase as compared to α phase. Locally around α–β interface, the stresses are considerably higher as compared to those in α and β. Higher stress values encountered in β phase are due to the higher yield stress of β phase as compared that off α. There are also isolated regions of very high stress concentration (shown by red colour) especially where the α particles meet. Particularly, these regions of high stress concentration are obtained near the locations where two α particles meet in certain orientations (Fig. 7b, shown by single arrow) and interestingly there are far off (Fig. 7b, shown by double arrow), there is a region of high stress concentrations. This is important from the tensile behaviour point of view as these will act as crack or void nucleation sites.

An elastic strain map is shown in Fig. 7c. The elastic strain plot is also shows the same results as of stress map. The plastic deformation maps are shown in Fig. 7d in this case α phase deforms more than β. Also there are α particles especially in the middle which appears to deform more than those in the periphery. Higher plastic strain in α phase is expected since α phase is considerably softer (Fig. 3). Then one can notice the strain incompatibility across α–β interface and there these regions are prone to void formation or cracking. This is consistent with the stress mapping except that the stress concentration occurs for certain orientations of α. Nevertheless, the fact that α–β interface are crack or void nucleation sites is further confirmed by observations of Mahajan and Margolin [21] also showed that slip starts at softer α phase (consistent with strain map in the investigation) and incompatibility between α and β results in cracking at the interface at strain values as low as 0.2%.

The stress values in α and β ranges from 300 MPa to 475 MPa and 475 MPa to 880 MPa (Fig. 7b). Whereas, strain in these phases ranging from 0.0013 to 0.012 and 0 to 0.0013 (Fig. 7d). It is clearly seen that the strain inhomogeneity can be an order of magnitude as a opposed to the significantly less variation in the stress values (at the most by a factor of 2). Hence, a constant stress behaviour.

3.4. Effect of α particle size on the stress–strain curve

Figs. 2, 4a and 4b represent respectively the finest, the medium and the coarser of α particle 2D FEM models. In all these three models the volume fraction of α (16%), numbers of triangular elements, number of nodes is constant. Same boundary conditions and loads are applied in order to get the stress–strain curve. After the simulation, the stress–strain curves are developed for all the three α grain sizes (Fig. 8). As the α particle size increases, the stress–strain curve is shifted down.

3.5. The analysis of the distribution of the stress and strain of the titanium alloy for different α particle sizes

Displacement plots are depicted in Fig. 9 at 0.83% strain (0.05 mm displacement). The stress and elastic strain maps for different particle size are shown in Figs. 10 and 11 respectively. The stress concentration points increase with increase in particle size. For the largest particle size, there are regions with very high stress concentration (shown in red[1]). Plastic strain maps (Fig. 12) show that with increase in plastic strain the deformation level in α increases. Additionally, for high plastic strain some α particles appear to heavily deform especially near the periphery.

The increase in stress value at a constant plastic strain with decreasing α particle size (volume fraction is constant) can be

[1] Please note that Figs. 10 and 11 will appear in B/W in print and color in the web version. Based on this, please approve the footnote 1 which explains this.

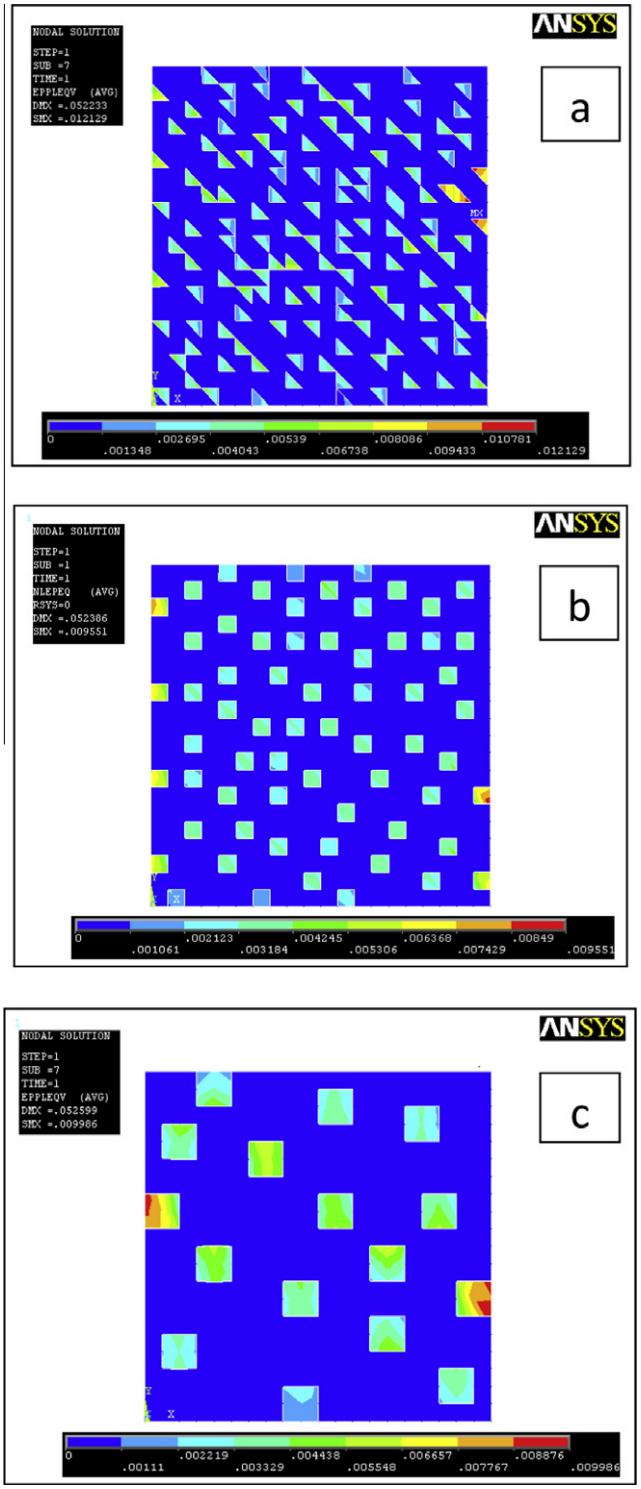

Fig. 12. VonMises plastic strain distributions at 0.83% strain for (a) finer, (b) medium and (c) coarser α grain sizes.

explained by examining closely the strain map (Fig. 12). For the finest α particle, the strain in α is larger than that in β, the deformation is more homogeneous (Fig. 12). Also, the strain difference in between α and β is less (the average strain in α is 0.001–0.003 and that in β is 0–0.001). On the other hand, the strain difference is fairly large (the average strain in α is 0.003–0.006 and that in β is 0–0.001) for coarser particle (Fig. 12). Thus, it is clearly observed that the finer particles may be able induce more deformation in β because of their uniform distribution and lower strain differential. This in turn will result in higher strength. An explanation on similar lines has been offered by Ankem et al. [19].

As regards stress concentration, it is seen that stress concentration points are more in coarser particle size distributions (Fig. 10). This confirms the conventional knowledge, the fine size particle distribution is always preferable because stress and strain homogeneity. Another interesting point is the stress concentration regions are located at an angle of 45° especially for coarse particle size distributions.

4. Conclusions

From this study, it can be concluded that:

(1) The measured stress–strain curve of Ti–10V–4.5Fe–3Al (16% volume fraction of α) closely fits the simulated one based on the stress–strain curves of individual phases both α and β (average error 6.22% and $R = 0.98$).
(2) The finite element model used in this attempt is acceptable and can be used for further simulation to analyse the effect of factors and discuss the distributions of micro-stress and micro-strain of the alloy.
(3) The stresses in β are more as compared that of the stresses in α, on the other hand the strain in α is more when compared to the strain β phase for a particular load.
(4) As the α particle size increases, the stress–strain curve is shifted down.
(5) The stress concentration points increase with increase in particle size. For the largest particle size, there are regions with very high stress concentration.
(6) Finer particles may able induce more deformation in β because of their uniform distribution and lower strain differential

References

[1] Moiseyev Valentin N. Titanium alloys: Russian aircraft and aerospace applications. 1st ed. CRC Press; 2005.
[2] Boyer RR. An overview on the use of titanium in the aerospace industry. Mater Sci Eng A 1996;213:103–14.
[3] Yamada Makoto. An overview on the development of titanium alloys for non-aerospace application in Japan. Mater Sci Eng A 1996;213:8–15.
[4] Eylon D. In: Fujishiro Shiro, Eylon D, Kishi T, editors. Metallurgy and technology of practical titanium alloys. Warrendale (PA): TMS; 1994. p. 29–36.
[5] Bania PJ. In: Eylon D, Boyer RR, Koss DA, editors. Beta titanium alloys in 1990s. Warrendale (PA): TMS; 1993. p. 3–14.
[6] Bania PJ, Hutt AJ, Adams RE, Parris WM. In: Froes FH, Caplan KL, editors. Titanium '92 science and technology. TMS; 1993. p. 2787–94.
[7] Singh AK, Bhattacharjee Amit, Gogia AK. Microstructure and texture of rolled and annealed b titanium alloy Ti–10V–4.5Fe–1.5Al. Mater Sci Eng A 1999;270:225–30.
[8] Gunawarmana B, Niinomi Mitsuo, Akahori Toshikazu, Souma Takayuki, Ikeda Masahiko, Toda Hiroyuki. Mechanical properties and microstructures of low cost β titanium alloys for healthcare applications. Mater Sci Eng C 2005;25:304–11.
[9] Balasubrahmanyam VV, Prasad YVRK. Deformation behaviour of beta titanium alloy Ti–10V–4.5Fe–1.5Al in hot upset forging. Mater Sci Eng A 2002;336:150–8.
[10] Bhattacharjee A, Ghosal P, Gogia AK, Bhargava S, Kamata SV. Room temperature plastic flow behaviour of Ti–6.8Mo–4.5Fe–1.5Al and Ti–10V–4.5Fe–1.5Al: effect of grain size and strain rate. Mater Sci Eng A 2007;452–453:219–27.
[11] Zhao Xiqing, Zang Xinliang, Wang Qingfeng, Park Joongkeun, Yang Qingxiang. Numerical simulation of the stress–strain curve and the stress and strain distributions of the titanium-duplex alloy. Rare Metals 2008;27(5):463.
[12] Kosec B, Kampus Z, Kosec L, Kosel F. Macroscopic modelling and simulation of two-phase copper matrix materials subjected to tensile deformation. J Acheive Mater Manuf Eng 2006;15(1–2):114–9.
[13] Ziaja W. Finite element modelling of the fracture behaviour of surface treated Ti–6Al–4V alloy. Arch Comput Mater Sci Surf Eng 2009;1(1):53–60.

[14] Ankem Sreeramamurthy, Margolin Harold, Greene Charles A, Neuberger Brett W, Gregory Oberson P. Mechanical properties of alloys consisting of two ductile phases. Progr Mater Sci 2006;51:632–709.
[15] He Xiaoming, Yu Zhongqi, Liu Guiming, Wang Wenge, Lai Xinmin. Mathematical modeling for high temperature flow behavior of as-cast Ti–45Al–85Nb–(W, B, Y) alloy. Mater Des 2009;30:166–9.
[16] Liao Bo, Zhang ChunLing, Wu Jing, Cai Dayong, Zhao Chunmei, Ren Xuejun, et al. Numerical simulation of the stress–strain curve of duplex weathering steel. Mater Des 2008;29:562–7.
[17] Jinoch Jindrich, Ankem Sreeramamurthy, Margolin Harold. Calculations of stress–strain curve and stress and strain distributions for an α–β Ti–8Mn alloy. Mater Sci Eng 1978;34:203–11.
[18] Yolton CF, Froes FH, Malone RF. Alloy elements effects in. metastable Titanium alloy. Met Trans A 1979;10:132–4.
[19] Ankem Sreeramamurthy, Margolin Harold. Finite Element Method (FEM) calculations of stress–strain behaviour of alpha–beta Ti–Mn alloys: Part I. Stress–strain relations. Metall Trans A 1982;13A:595–601.
[20] Dong Hai-feng, Li Jing, Zhang Yue, Park Joongkeun, Yang Qing-xiang. Numerical simulation on the micro-stress and micro-strain of low Si–Mn–Nb dual-phase steel. Int J Miner, Metall Mater 2010;17(2):173–8.
[21] Mahajan Y, Margolin H. Surface cracking in alpha–beta Titanium alloys under unidirectional loading. Metall Trans A 1978;9(3):427–31. 48.